THE ASTROPHYSICAL JOURNAL, 477:8–20, 1997 March 1

PHOTOIONIZATION, NUMERICAL RESOLUTION, AND GALAXY FORMATION

DAVID H. WEINBERG
Ohio State University, Department of Astronomy, Columbus, OH 43210; dhw@payne.mps.ohio-state.edu
LARS HERNQUIST[1]
University of California, Lick Observatory, Santa Cruz, CA 95064; lars@helios.ucsc.edu
AND
NEAL KATZ
University of Washington, Department of Astronomy, Seattle, WA 98195; nsk@astro.washington.edu
Received 1996 April 16; accepted 1996 September 19

ABSTRACT

Using cosmological simulations that incorporate gasdynamics and gravitational forces, we investigate the influence of photoionization by an ultraviolet radiation background on the formation of galaxies. In our highest resolution simulations, we find that photoionization has essentially no effect on the baryonic mass function of galaxies at $z = 2$, down to our resolution limit of $\sim 5 \times 10^9\ M_\odot$. We do, however, find a strong interplay between the mass resolution of a simulation and the microphysics included in the computation of heating and cooling rates. At low resolution, a photoionizing background can appear to suppress the formation of even relatively massive galaxies. However, when the same initial conditions are evolved with a factor of 8 improvement in mass resolution, this effect disappears. Our results demonstrate the need for care in interpreting the results of cosmological simulations that incorporate hydrodynamics and radiation physics. For example, we conclude that a simulation with limited resolution may yield more accurate results if it ignores some relevant physical processes, such as photoionization. At higher resolution, the simulated population of massive galaxies is insensitive to the treatment of photoionization or the inclusion of star formation in the simulations, but it does depend significantly on the amplitude of the initial density fluctuations. By $z = 2$, an $\Omega = 1$ cold dark matter model normalized to produce the observed masses of present-day clusters has already formed galaxies with baryon masses exceeding $10^{11}\ M_\odot$.

Subject headings: galaxies: formation — galaxies: luminosity function, mass function — hydrodynamics — methods: numerical — radiative transfer

1. INTRODUCTION

Hierarchical models of structure formation, in which small-scale perturbations collapse gravitationally and merge into progressively larger objects, offer an attractive theoretical setting for galaxy formation. As first emphasized by White & Rees (1978), the dissipation of the gas component inside dark matter halos can explain the gap between the masses of large galaxies and the masses of rich clusters, and the combination of cooling arguments with the formation and merger history of the dark halos allows a prediction of the baryonic mass function of galaxies. The White & Rees picture of galaxy formation fits naturally into the more encompassing inflation plus cold dark matter (CDM) theory (Peebles 1982; Blumenthal et al. 1984) and its variants involving a cosmological constant, space curvature, or an admixture of hot dark matter. However, attempts to predict the galaxy luminosity function in such scenarios, using analytic and semianalytic extensions of the Press & Schechter (1974) formalism, have revealed a persistent difficulty: these hierarchical models predict an abundance of faint galaxies that far exceeds that in most estimates of the galaxy luminosity function (e.g., White & Frenk 1991; Kauffmann, White, & Guideroni 1993; Cole et al. 1994; Heyl et al. 1995). This defect is of great interest since it could undermine not just specific cosmological models but the entire class of hierarchical theories of galaxy formation.

Various ideas have been proposed to overcome this "faint galaxy excess" problem, including feedback from star formation (e.g., Dekel & Silk 1986; Cole 1991; Lacey & Silk 1991; White & Frenk 1991), preheating of the intergalactic medium (e.g., Blanchard, Valls-Gabaud, & Mamon 1992; Tegmark, Silk, & Evrard 1993), and the possibility that faint galaxies are present in the real universe but are undercounted in most surveys because of their low surface brightness (e.g., Ferguson & McGaugh 1995). Efstathiou (1992; see also Ikeuchi 1986; Rees 1986; Babul & Rees 1992) suggested that the formation of low-mass galaxies might instead be suppressed by photoionization from an ultraviolet (UV) radiation background, which can heat diffuse gas to temperatures of a few $\times 10^4$ K and eliminate the dominant sources of atomic cooling at temperatures below 5×10^5 K. The photoionization solution is an attractive one because the observed quasars alone should produce a rather strong UV background at redshifts $z \sim 2$–4 and massive star formation in young galaxies would only increase the effect. In an isolated, coherent collapse, one expects the influence of photoionization to be small for objects with virial temperatures above $\sim 5 \times 10^5$ K since at these temperatures primordial composition gas is highly ionized by collisions alone. However, in a hierarchical scenario galaxies form by mergers of smaller subunits, and processes that affect these subunits may be able to percolate their influence to larger mass scales.

In this paper, we examine the effects of photoionization on galaxy formation using three-dimensional simulations that follow the evolution of gas and dark matter in an

[1] Sloan Fellow, Presidential Faculty Fellow.

expanding universe. Our simulations use TreeSPH (Hernquist & Katz 1989; Katz, Weinberg, & Hernquist 1996, hereafter KWH), a code that combines smoothed particle hydrodynamics (SPH; see, e.g., Lucy 1977; Gingold & Monaghan 1977; Monaghan 1992) with a hierarchical tree method for computing gravitational forces (Barnes & Hut 1986; Hernquist 1987) in a periodic volume (Bouchet & Hernquist 1988; Hernquist, Bouchet, & Suto 1991). This numerical treatment avoids the physical idealizations required in Efstathiou's (1992) semianalytic treatment which made his quantitative conclusions rather uncertain. Our simulation volume is large enough to contain many galaxies embedded in an appropriate large-scale environment, so our analysis complements the numerical studies of Steinmetz (1995), Quinn, Katz, & Efstathiou (1996, hereafter QKE), Thoul & Weinberg (1996, hereafter TW), Navarro & Steinmetz (1996) which examine collapses of individual objects with higher resolution (see discussion in § 5).

The middle phrase of our tripartite title may seem out of place: photoionization is a *physical* process that might plausibly influence galaxy formation, but numerical resolution is not. However, numerical resolution can have a critical effect on simulations of galaxy formation. Furthermore, the interaction between resolution and assumptions about gas microphysics (photoionization in particular) can be quite subtle. To demonstrate these points, it is most revealing to describe our results in the order in which we obtained them. After summarizing the physical effects of photoionization in § 2, we first present results from a series of low-resolution simulations in § 3, then move to high-resolution simulations in § 4. In § 5 we discuss the implications of our results for numerical simulations and for the "faint galaxy" problem.

2. PHOTOIONIZATION AND COOLING RATES

As emphasized by Efstathiou (1992) and TW, a photoionizing background field can have at least two important effects on gas that would otherwise cool and collapse into galaxies. First, heating the gas may stabilize it against gravitational collapse, preventing it from falling into shallow dark matter potential wells. Second, an ionizing background can greatly lengthen cooling times, making it impossible for gas to dissipate the thermal energy generated by collapse and cool to temperatures and densities at which star formation can occur. Figures 1 and 2 illustrate these effects. Figure 1 shows the cooling rate as a function of temperature for primordial composition gas, 76% hydrogen and 24% helium by mass, with no ionizing background. Abundances of ionic species are computed assuming collisional equilibrium, i.e., that the rate at which any species is destroyed by collisional ionization or recombination is equal to the rate at which it is created by collisional ionization or recombination of other species. In this approximation, relative abundances depend only on temperature, and because the cooling is dominated by two-body processes, the cooling rate at fixed temperature is simply proportional to the square of the gas density. In Figure 1, $n_{\rm H}$ is the number density of hydrogen nuclei: $n_{\rm H} \equiv X\rho_{\rm gas}/m_p$, where $X = 0.76$ is the hydrogen fraction. In a cosmological context,

$$n_{\rm H} = 2.3 \times 10^{-6}\left(\frac{X}{0.76}\right)\left(\frac{1+z}{3}\right)^3\left(\frac{\Omega_b h^2}{0.01}\right)\frac{\rho}{\bar{\rho}}\ {\rm cm}^{-3}\ , \quad (1)$$

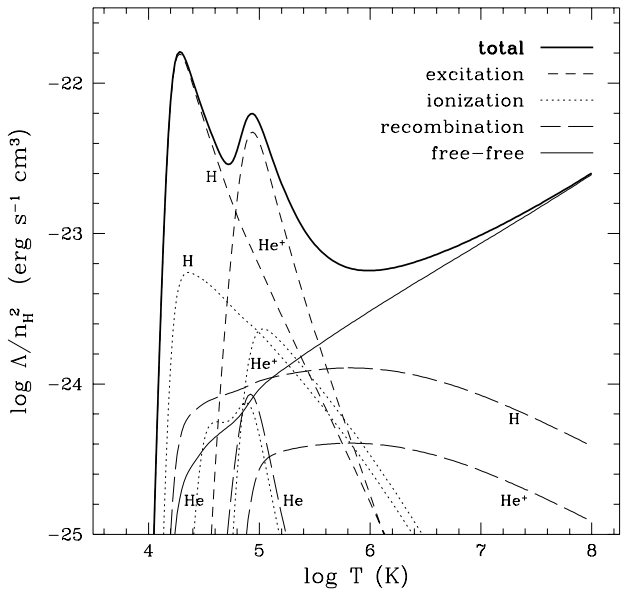

FIG. 1.—Cooling rates as a function of temperature for a primordial composition gas in collisional equilibrium. The heavy solid line shows the total cooling rate. The cooling is dominated by collisional excitation (*short-dashed lines*) at low temperatures and by free-free emission (*thin solid line*) at high temperatures. Long-dashed lines and dotted lines show the contributions of recombination and collisional ionization, respectively.

where Ω_b is the baryon density parameter, $h \equiv H_0/100$ km s^{-1} Mpc^{-1}, and $\rho/\bar{\rho}$ is the ratio of the local gas density to the average gas density.

The ionization, recombination, and cooling rates used for Figure 1 are taken primarily from Black (1981) and Cen (1992); the full set of adopted rates and abundance equations appears in KWH. At low ($T \sim 2 \times 10^4$ K) and moderate ($T \sim 10^5$ K) temperatures, cooling is dominated by collisional excitations of hydrogen and singly ionized helium, respectively. At $T > 10^6$ K, the gas is almost fully ionized, and free-free emission dominates. At $T < 10^4$ K, the gas is entirely neutral and collisions are too weak to produce excitation, so the cooling rate is essentially zero. (Molecular cooling can become significant at very high densities, but we ignore it here.)

An ultraviolet background can radically alter this picture of cooling because photoionization dominates over collisional ionization in cold, low-density gas. Relative abundances depend on density, so the cooling rate is no longer strictly proportional to $n_{\rm H}^2$. One can nonetheless compute a "cooling curve" like Figure 1 for any specified density and UV background spectrum by assuming ionization equilibrium, a balance between destruction and ionization rates with photoionization taken into account (see KWH for details). While ionization equilibrium does not hold during the epoch of reionization itself, it is thereafter an excellent approximation under most cosmologically relevant conditions (Vedel, Hellsten, & Sommer-Larsen 1994). Figure 2 shows cooling curves for $n_{\rm H} = 10^{-6}$, 10^{-4}, 10^{-3}, and 10^{-2} cm^{-3} and a UV background

$$J(\nu) = J_0\left(\frac{\nu}{\nu_0}\right)^{-\alpha}\ {\rm ergs\ s^{-1}\ cm^{-2}\ sr^{-1}\ Hz^{-1}}\ , \quad (2)$$

with $\alpha = 1$ and J_0, the intensity at the Lyman limit frequency ν_0 in units of ergs s^{-1} cm^{-2} sr^{-1} Hz^{-1}, is equal to 10^{-22}. At low densities, the UV background photoionizes

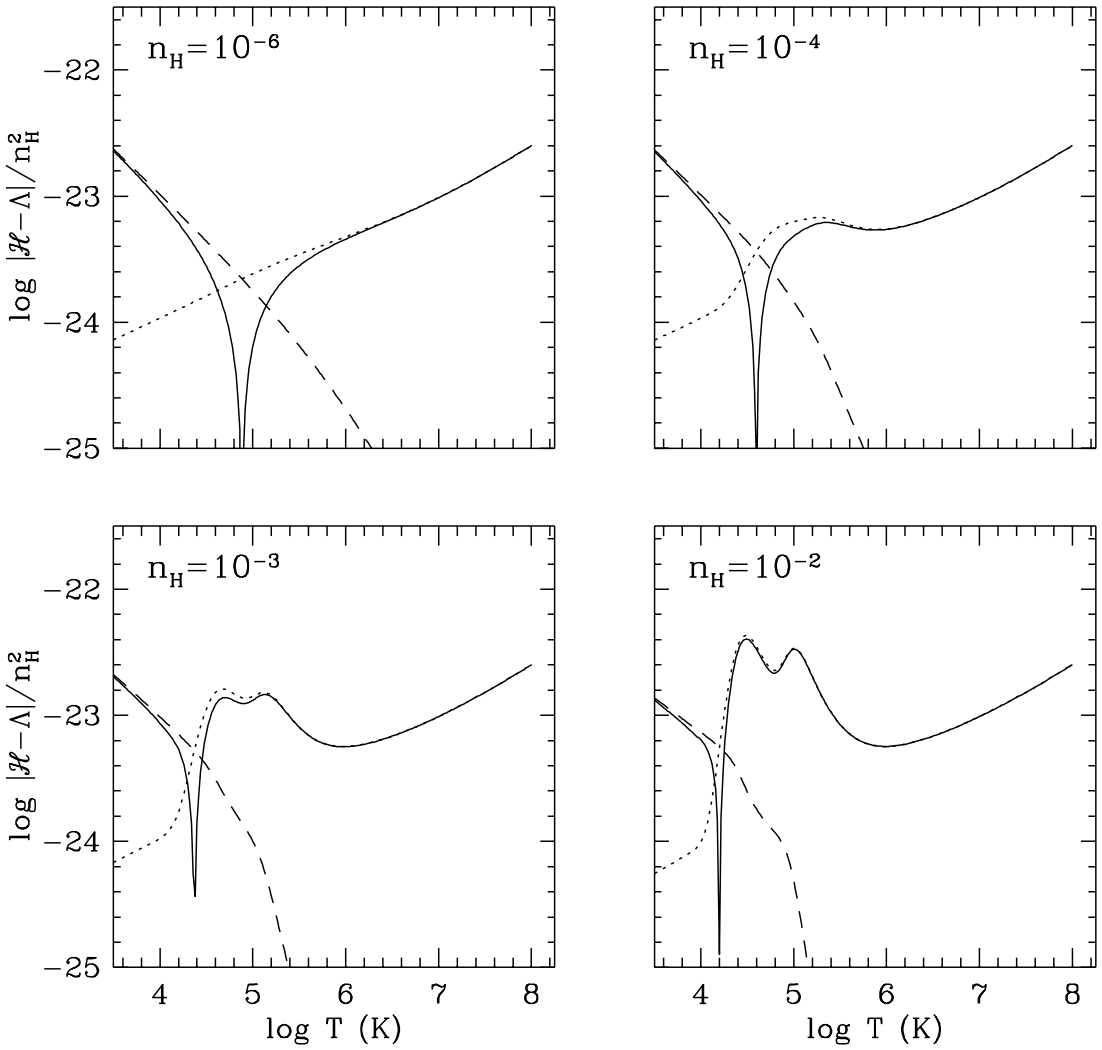

FIG. 2.—Net cooling rates as a function of temperature for a primordial composition gas in ionization equilibrium with a UV radiation background of intensity $J(\nu) = 10^{-22}(\nu_0/\nu)$ ergs s^{-1} cm^{-2} sr^{-1} Hz^{-1}, for hydrogen densities $n_H = 10^{-6}$, 10^{-4}, 10^{-3}, and 10^{-2} cm^{-3}. In each panel, the dotted line shows the cooling rate and the dashed line shows the rate of heating by photoionization. The solid curve shows the absolute value of the net cooling rate; heating dominates at low temperatures and cooling at high temperatures.

the hydrogen and helium, eliminating the excitation processes that dominate Figure 1 between 10^4 and 3×10^5 K. Furthermore, the residual energy of photoelectrons heats the gas, and at low temperatures heating exceeds cooling. In Figure 2, dotted lines show cooling rates, dashed lines heating rates, and solid lines the net cooling (or heating) rate $|\mathscr{H} - \Lambda|$. This net rate goes to zero at the temperature T_{eq} where the gas would reach radiative thermal equilibrium with the background, if other heating and cooling processes were unimportant. However, unlike ionization equilibrium, thermal equilibrium is rarely a good approximation under cosmological conditions, and in our numerical simulations we always integrate the thermal energy equation for each gas particle, using ionization equilibrium only to compute radiative cooling and heating rates as a function of density and temperature.

As the gas density increases, recombination begins to win out over photoionization. The hydrogen and helium excitation bumps reappear, and the cooling curve gradually returns to the collisional equilibrium form of Figure 1. At low densities (e.g., $n_H < 10^{-6}$ cm^{-3} for the UV background used in Fig. 1) the gas is almost fully ionized, and the curve $|\mathscr{H} - \Lambda|/n_H^2$ again becomes independent of density. The cooling processes in this regime, recombination and free-free emission, are proportional to n_H^2 when the gas is fully ionized. The rate of photoelectric heating off the residual neutral atoms (and singly ionized helium atoms) is proportional to the densities of neutral (and singly ionized) atoms, which are themselves proportional to the recombination rates and hence to n_H^2.

Changes in the UV background have predictable effects on the cooling curve. Altering the intensity J_0 is equivalent to rescaling the gas density, e.g., with $\alpha = 1$ and $J_0 = 10^{-21}$, Figure 1 would be exactly the same except that the $n_H = 10^{-6}$ cm^{-3} curve would now correspond to $n_H = 10^{-5}$ cm^{-3}, 10^{-4} to 10^{-3}, and so forth. If J_0 is kept fixed but the spectral *shape* is softened (e.g., $\alpha = 5$ instead of $\alpha = 1$), then helium is photoionized less frequently than hydrogen, and the helium excitation bump returns more quickly than the hydrogen bump as density increases. In addition, the typical photoionization event is less energetic, so the heating rate and equilibrium temperature both drop. Some of these effects are illustrated in the cooling curves of Efstathiou (1992) and TW.

The effects of photoionization on cooling of primordial gas are easily summarized. In low-density gas, photoioniza-

tion injects energy and eliminates the mechanisms that dominate cooling at moderate temperatures. The result can be an order-of-magnitude reduction in the cooling rate at temperatures as high as 2×10^5 K and a reversal of sign, from cooling to heating, at somewhat lower temperatures. These effects gradually become unimportant as the gas density increases. At $T > 10^6$ K, gas is fully ionized by collisions alone, and photoionization has no impact on cooling rates.

3. LOW-RESOLUTION SIMULATIONS

We began our study of photoionization by performing a set of low-resolution simulations similar to those described by Katz, Hernquist, & Weinberg (1992, hereafter KHW) and Hernquist, Katz, & Weinberg (1995) but including UV background fields of various intensities and spectral indices. In all cases, we model the evolution of a periodic region in a standard cold dark matter universe, with $\Omega = 1$, $h = 0.5$, and a baryon fraction $\Omega_b = 0.05$. We normalize the CDM power spectrum so that the rms mass fluctuation in spheres of radius $8h^{-1}$ Mpc is $\sigma_8 = 0.7$ at redshift zero. This normalization yields a good match to the measured masses of rich galaxy clusters (White, Efstathiou, & Frenk 1993), but when the spectrum is extrapolated to large scales it underproduces the level of microwave background anisotropies observed by *COBE* (Smoot et al. 1992; Bunn, Scott, & White 1995). In this paper we are interested in generic physical effects in a hierarchical clustering theory of galaxy formation, not in the detailed predictions of a particular CDM model, so a normalization that produces the appropriate level of clustering on the scales of galaxy groups and clusters is better suited to our purposes.

In all cases our simulation volume is a cube of comoving size 22.22 Mpc. Our low-resolution models employ 32^3 gas and 32^3 dark matter particles, implying a mass per particle of $1.2 \times 10^9\ M_\odot$ and $2.2 \times 10^{10}\ M_\odot$ for the gas and dark matter, respectively. The simulations are evolved with TreeSPH, using a fixed time step for the dark matter particles of $\Delta t_d = t_0/4000$, where $t_0 = 2/(3H_0)$. The time steps for the gas particles, Δt_g, are allowed to vary by powers of 2 so that the gas locally satisfies the Courant condition, with the constraint that Δt_g is always smaller than or equal to Δt_d. Spatial resolution is determined by the gravitational softening length, ϵ, which is 20 comoving kpc (13 kpc equivalent Plummer softening) and by the smoothing lengths of the gas particles, which are updated continuously so that each smoothing volume contains 32 neighbors. To improve efficiency, we do not allow any smoothing length to drop below $\epsilon/4$, which implies that smoothed estimates for some particles in very overdense regions are calculated with more than 32 neighbors (see, e.g., Evrard 1988; KWH). We include the effects of both Compton and radiative cooling.

Aside from an imposed floor on the gas particle smoothing lengths, the simulation with $J(\nu) = 0$ described in this section is identical in all respects to that in KHW, except that here we include gas dynamical effects all the way to redshift zero instead of converting the gas to collisionless matter at $z = 0.375$. (The smoothing floor itself has virtually no effect on the results.) We also ran four low-resolution simulations with an ionizing background for various combinations of the parameters J_0 and α. Specifically, for each of the choices $J_0 = 10^{-21}$ and 10^{-22} we consider spectral indices $\alpha = 1$ and $\alpha = 5$, for a total of four additional simulations. In all cases, we multiply the overall intensity of the background by the redshift-dependent factor

$$F(z) = \begin{cases} 0\ , & \text{if } z > 6\ ; \\ 4/(1+z)\ , & \text{if } 3 \le z \le 6\ ; \\ 1\ , & \text{if } 2 < z < 3\ ; \\ [(1+z)/3]^3\ , & \text{if } z < 2\ . \end{cases} \tag{3}$$

While the detailed form of this evolution is somewhat arbitrary, it reflects the fact that the population of quasars, the likely source of much of the UV background, peaks at redshifts of 2–3 and declines toward higher and lower redshifts.

In these simulations, gravitational instability collects the dark matter and gas into a network of sheets, filaments, and clumps, interwoven with low-density tunnels and rounded voids (see, e.g., Fig. 1 of KHW). The combination of heating and cooling mechanisms leads to a three-phase structure in the gas distribution. The gas in voids has low density and is either warm or cold depending on whether an ionizing background is included. The gas in overdense regions consists of extremely dense, radiatively cooled lumps close to the equilibrium temperature $T_{\rm eq}$, orbiting within halos of moderately dense, shock heated material, typically at X-ray emitting temperatures.

These features are illustrated in Figure 3, where we plot the temperatures and densities of all the gas particles at redshifts $z = 2$, 0.5, and 0, for a simulation with no ionizing background ($J_0 = 0$) and a simulation with a radiation field of intensity $J_0 = 10^{-22}$ and spectral index $\alpha = 5$. In the no-background model, the clump of particles centered on $\log T \approx 1$ and $\rho \approx \rho_b$ at $z = 2$ represents the cold gas in the underdense regions. This material continues to cool adiabatically as the universe expands (and as voids grow in comoving volume), and by $z = 0$ these particles are so cold that they no longer appear in the bottom left panel of Figure 3. The hot, X-ray emitting gas phase consists of the particles in Figure 3 at $\log T \gtrsim 5.5$ and typical overdensities of 10–1000. The amount of this material increases with time as more and more gas falls into deep potential wells and is shock heated. The third phase, the dense, cool globs of gas that we associate with forming galaxies, resides in the thin "ridge" of particles lying at temperatures around 10^4 K and extending to overdensities of nearly 10^9. (Note, however, that dynamics are not accurately resolved at overdensities above 10^6 or so because of gravitational softening.) The amount of very dense gas increases with time as new material cools and condenses into galaxies.

In broad terms, the evolution of the gas in the photoionized simulation is similar to that in the no-background simulation, but there are two key differences. As is clearly visible in Figure 3, the low-density gas in the underdense regions cannot cool to arbitrarily low temperatures since photoelectric heating steadily injects energy. Nearly all of this gas remains ionized and resides at temperatures between 10^3 and 10^4 K, occupying a locus where photoelectric heating balances adiabatic cooling. The other important difference between the two simulations, not so immediately obvious from Figure 3, is that the amount of gas in the very dense globs is greatly reduced when the UV background field is included. This difference suggests that an ionizing background could seriously influence the formation of even relatively massive galaxies.

To further investigate this last possibility, we identified potential sites of galaxy formation in each of our low-resolution simulations using an adaptive version of the

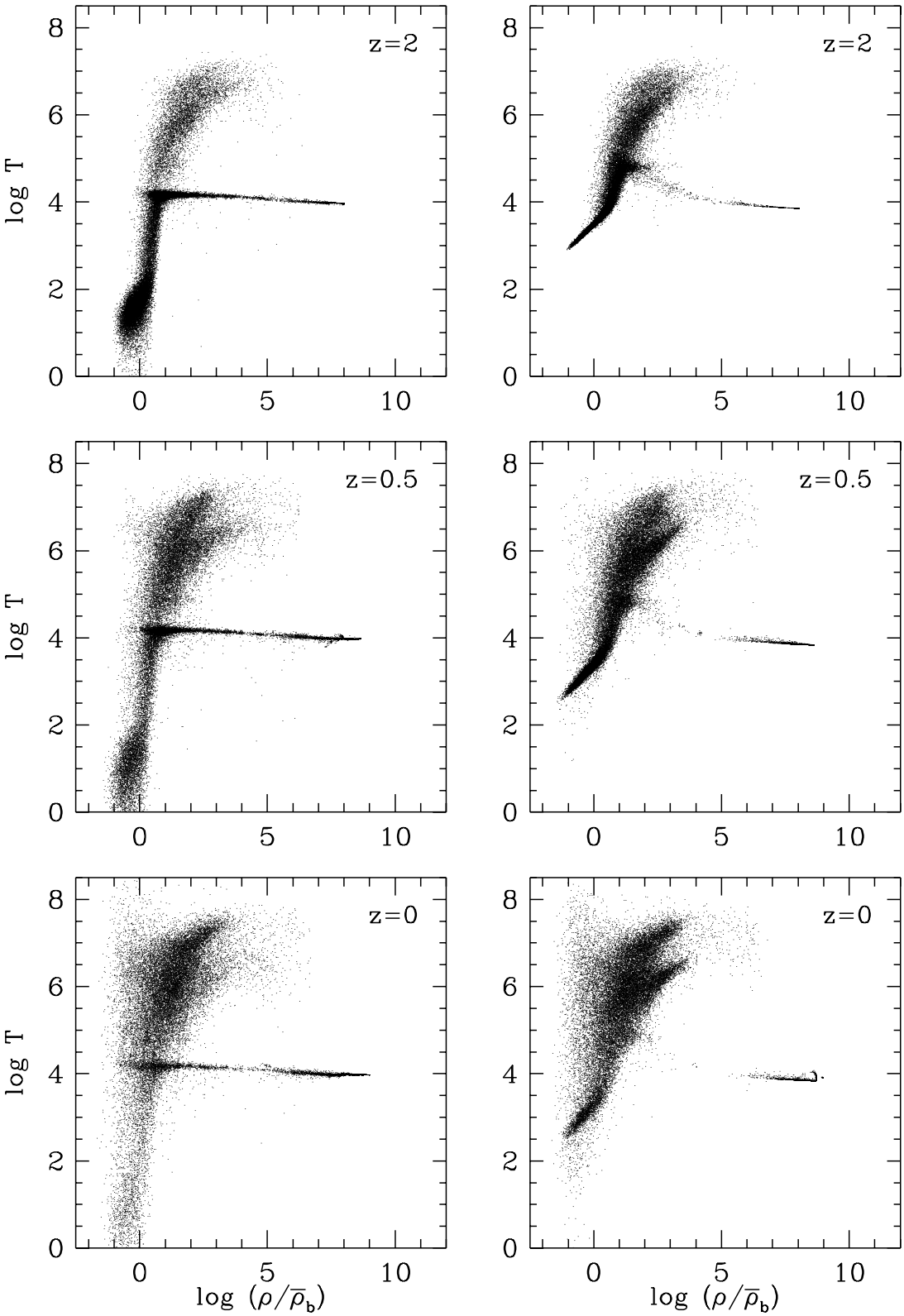

FIG. 3.—Distribution of gas in the density-temperature plane in simulations with (*right*) and without (*left*) an ionizing background. Redshifts $z = 2$, 0.5, and 0, are shown from top to bottom. Each point represents a single gas particle; temperatures are in degrees Kelvin and densities are scaled to the mean baryon density.

DENMAX algorithm formulated by Gelb & Bertschinger (1994a, 1994b). Our new method (SKID; for the code and a description of its operation see http://www-hpcc.astro.washington.edu/tools), employs the same general approach as DENMAX, associating particles with local-density maxima and identifying gravitationally bound groups. However, SKID computes densities and density gradients using spline kernel interpolation with a variable smoothing length instead of a grid of uniform cell spacing. To create a "galaxy" catalog, we select particles with

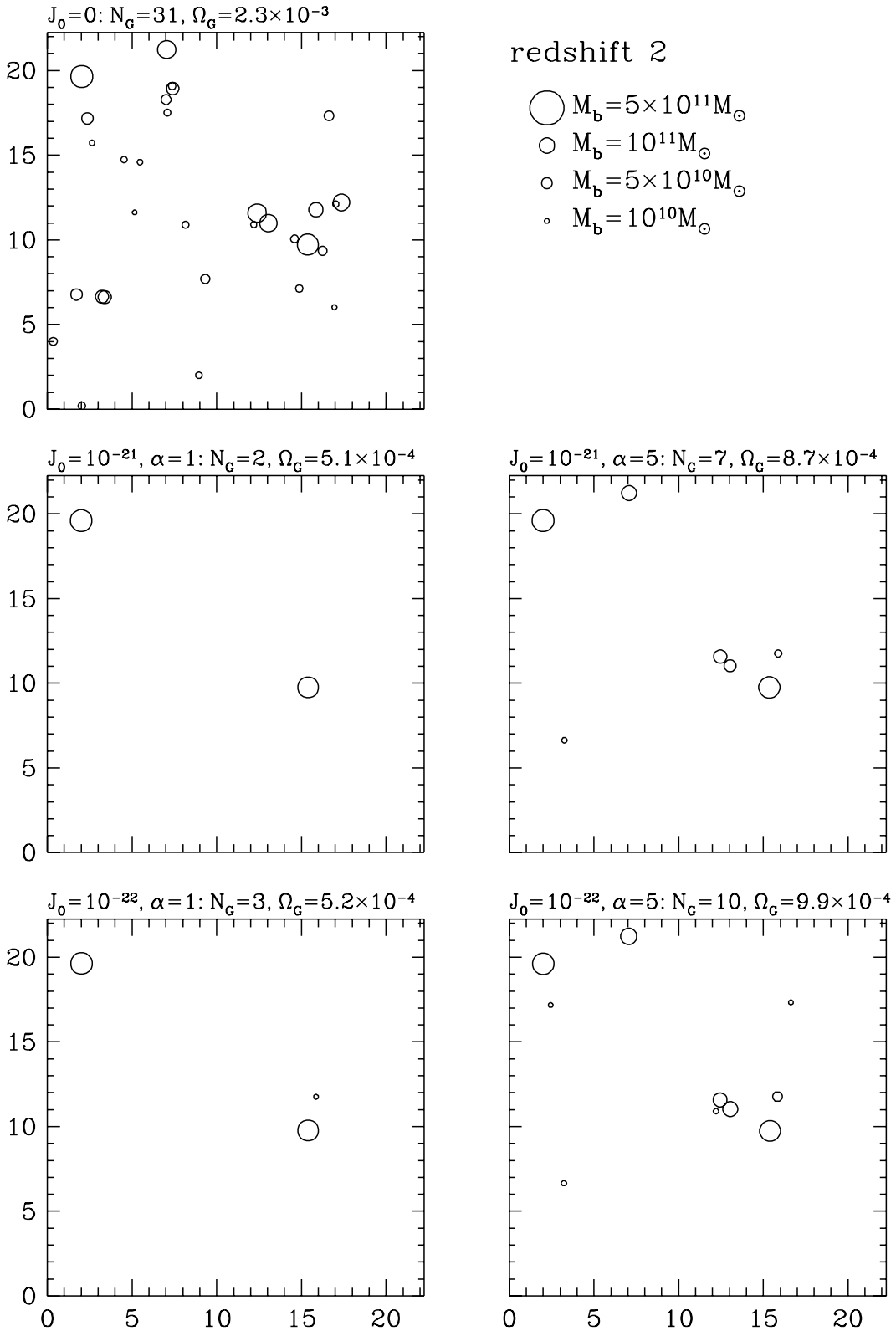

FIG. 4.—Galaxy distributions at $z = 2$. Each panel shows a projection of the 22 Mpc (comoving) simulation box; galaxies are represented by circles the area of which is proportional to their baryonic mass. The ionizing background parameters, number of galaxies, and value of Ω_G are indicated above each panel. The low-mass galaxies in the simulation without ionization (*top left*) are mostly absent from the simulations with an ionizing background.

$\rho_b/\bar{\rho}_b > 1000$ and $T < 30{,}000$ K and allow SKID to separate them into gravitationally bound objects. (Kinetic energies are computed relative to the average velocity of the grouped particles, and potential energies include the contribution of any dark matter or hot gas within $2\epsilon = 40$ comoving kpc of the density maximum. See the web site for details.) Because this component of the gas is highly clumped, the galaxy population identified in this way is very

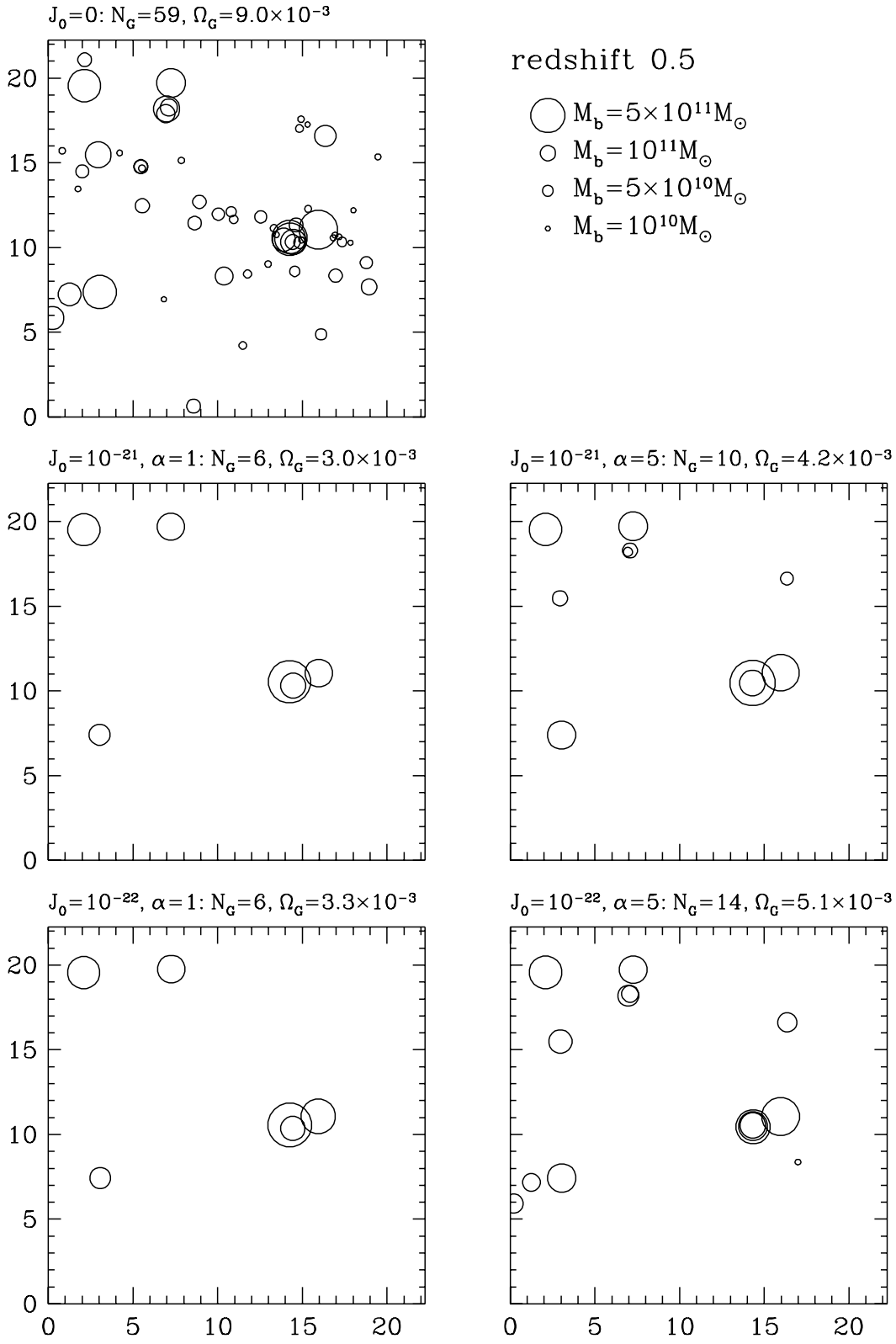

FIG. 5.—Same as Fig. 4 but at redshift $z = 0.5$

robust (see KWH). We retain all galaxies with eight or more bound members. Objects of this minimum mass are, of course, poorly resolved, although because SPH densities and temperatures are smoothed over 32 neighbors, even an eight-particle group must lie at the core of a more substantial gas concentration.

Figures 4 and 5 show the spatial distributions of the galaxies in these low-resolution simulations, at $z = 2$ and $z = 0.5$, respectively. Each galaxy is represented by a circle the area of which is proportional to its baryonic mass. The number of galaxies N_G and the mass fraction Ω_G of cold gas in galaxies are indicated above each panel.

Photoionization dramatically influences the formation of dense globs of gas in our low-resolution simulations. In all four cases with a background radiation field, the mass of cold, dense gas is greatly reduced compared to the no-background model. Few galaxies remain in any of the simulations with an ionizing background, and the amount of gas in this phase is reduced relative to that in the no-background model by up to a factor of 4.5 at $z = 2$. New galaxies continue to form at lower redshifts, but at $z = 0.5$ the number of galaxies remains a factor $\sim$4–10 lower, depending on J_0 and α. A comparison of the four cases indicates that the spectral index plays a more decisive role than the intensity in determining the suppression of galaxy formation. For example, the numbers and masses of galaxies in the two simulations with $\alpha = 1$ are nearly identical, while changing α to 5 restores some of the galaxies seen in the no-background model.

We originally interpreted the results shown in Figures 4 and 5 as evidence that photoionization by the UV background could suppress the formation of even relatively massive galaxies, with baryonic masses up to $M_b \sim 10^{11}$ $M_\odot$. Since the virial temperatures of such systems are above the level $T \sim 10^{5.5}$ K where photoionization significantly alters cooling rates (see Figs. 1 and 2), such an effect would have to be physically rather subtle, with photoionization either suppressing the formation of low-mass clumps that would otherwise merge into big galaxies or "hanging up" the cooling process at intermediate temperatures in the more massive systems, allowing the gas to be shock heated back to high temperatures in later mergers. Had these results been confirmed by higher resolution simulations, they would have implied that photoionization could easily solve the problem of an overabundance of low-mass galaxies in hierarchical clustering models. Indeed, the solution would be too good: unless the UV background spectrum were quite soft, it would be difficult to form any but the most massive galaxies, and the galaxy population would be sensitive to local variations in the UV background.

4. HIGH-RESOLUTION SIMULATIONS

While the sign of the effect indicated by Figures 4 and 5 seems physically plausible, the magnitude is quite surprising. We were therefore concerned that these results might be an artifact of our limited numerical resolution, and we decided to repeat two of the calculations at higher resolution, evolving only to $z = 2$ in order to avoid prohibitive computing costs. These simulations are identical in all respects to those with $J_0 = 0$ and with $J_0 = 10^{-22}$, $\alpha = 1$, except that they have eight times more gas and dark matter particles, $N = 64^3$ in each component. This change reduces the masses of individual gas and dark matter particles to 1.5×10^8 $M_\odot$ and 2.8×10^9 $M_\odot$, respectively. To ease comparison with the low-resolution simulations discussed above, we chose not to reduce the softening length, so that the spatial resolution is again limited to $\epsilon = 20$ kpc (comoving) in the computation of gravitational forces and to $\epsilon/4$ for smoothed estimates of hydrodynamic properties.

We repeated the analysis described in the preceding section to identify galaxies. Figure 6 shows the galaxy distributions at $z = 2$ in the simulations with $J_0 = 0$ (*bottom left*) and with $J_0 = 10^{-22}$, $\alpha = 1$ (*bottom right*). For reference, we replot the corresponding panels from Figure 4 for the low-resolution simulations (*top*).

Figure 6 demonstrates that the dramatic effect seen in the 32^3 particle simulations is indeed an artifact of limited mass resolution. The 64^3 particle simulations with and without a background radiation field are quite similar, both in the numbers of galaxies and in the total mass of gas contained in these galaxies. At $z = 2$, SKID identifies 403 galaxies in the no-background simulation and 353 galaxies in the simulation with an ionizing background. Virtually all galaxies with baryonic mass $M_b > 10^{10}$ $M_\odot$ in the no-background simulation have a counterpart in the photoionized simulation with nearly the same position and nearly the same mass. Some low-mass galaxies are absent in the photoionized simulation, and the value of Ω_G is reduced by about 10%. While the difference occurs in a mass range that is physically interesting, it may again be an artifact of limited resolution, now shifted to lower masses. In any event, this difference is much smaller than that seen in the two 32^3 simulations, where photoionization reduced the number of galaxies by a factor of 10 and the amount of cold gas by a factor of 4.4.

Figure 7 shows the cumulative mass functions of the galaxy populations from these four simulations. The two high-resolution simulations (*solid and dotted lines*) yield nearly identical mass functions, with a small offset produced by the absence of some low-mass galaxies in the photoionized model. The two low-resolution simulations (*dashed and dot-dashed lines*) differ dramatically from one another, having mass functions that coincide only at the highest masses. At masses $M_b \gtrsim 4 \times 10^{10}$ $M_\odot$, which corresponds to about 32 gas particles in the low-resolution simulations, the mass function of the low-resolution, no-background simulation agrees roughly with that of the two high-resolution simulations, although it is shifted slightly toward higher masses. Of course this simulation cannot reproduce the much lower mass systems formed in the high-resolution runs, but unlike the low-resolution photoionized simulation, its mass function is reasonably accurate down to its nominal resolution limit. This comparison suggests that a low-resolution simulation without photoionization can provide a useful guide to the behavior of a high-resolution run with photoionization, even though it omits a significant physical effect. We will return to this point in § 5.

From Figure 6, it is clear that most galaxies in the high-resolution, no-background simulation have a counterpart of similar mass in the photoionized simulation. To make this point explicitly, we match galaxies in the two simulations the positions of which agree to within 40 comoving kpc (twice the gravitational softening radius). We enforce one-to-one matches by ranking the two galaxy lists in order of decreasing baryonic mass and identifying each galaxy from the photoionized simulation with the most massive galaxy in the no-background simulation that lies within 40 kpc and has not yet been matched to a more massive galaxy. Of the 353 galaxies in the photoionized simulation, 334 find a counterpart by this procedure. Figure 8 plots the baryonic masses of matched galaxies in the two simulations against each other; crosses indicate unmatched galaxies. Nearly all the matched galaxies fall close to the diagonal line representing identical masses. There is a tendency for the galaxies in the no-background model to be slightly more massive than their counterparts in the photoionized model, but the effect is small and may be numerical rather than physical. The scatter is greater at lower masses, $M_b \lesssim 10^{9.5}$ $M_\odot$, corresponding to $N \lesssim 20$ particles. This effect could be numerical or physical, or it could instead reflect an inaccu-

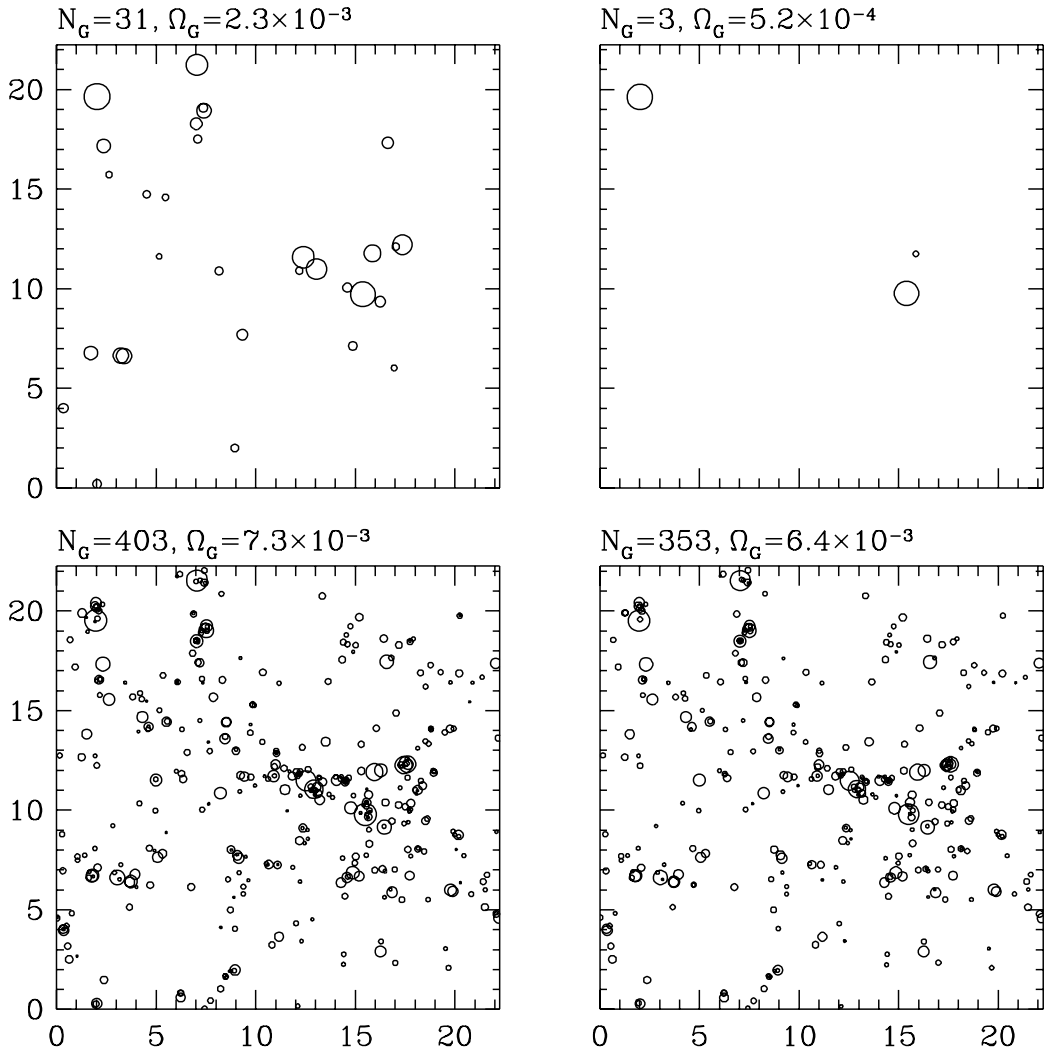

FIG. 6.—Galaxy distributions at $z = 2$ from low-resolution simulations (2×32^3 particles; *top*) and high-resolution simulations (2×64^3 particles; *bottom*), with no ionizing background (*left*) and with an ionizing background $J(\nu) = 10^{-22}(\nu_0/\nu)$ ergs^{-1} cm^{-2} sr^{-1} Hz^{-1} (*right*). The relation between circle area and galaxy baryon mass is the same as in Figure 4. The low-resolution simulations suggest that photoionization suppresses the formation of galaxies with baryonic masses below $\sim 10^{11}\ M_\odot$. The high-resolution simulations show that this suppression is a numerical artifact; with sufficient resolution, simulations with and without an ionizing background yield very similar galaxy populations.

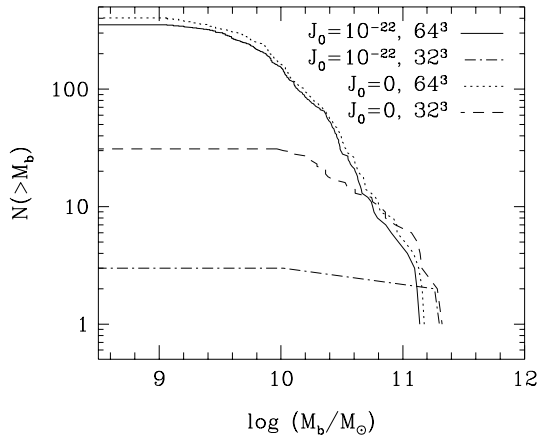

FIG. 7.—Cumulative galaxy baryonic mass functions at $z = 2$ for the four simulations shown in Figure 6. The two low-resolution simulations yield quite different mass functions, but the mass functions of the two high-resolution simulations are nearly identical.

racy in our matching scheme for the least massive objects.

The vast majority of the galaxies "missing" from the simulation with a background radiation field are of relatively low mass, with $M_b \lesssim 10^{9.5}\ M_\odot$. Given the lesson of our low-resolution experiments, we suspect that the absence of these least massive systems is a residual effect of finite mass resolution, and that simulations with still higher resolution would show an even closer match between the galaxy populations with and without photoionization.

5. DISCUSSION

We originally undertook this study in order to investigate the influence of a photoionizing background radiation field on galaxy formation and the intergalactic medium. Our low-resolution simulations offered a tantalizing hint that photoionization could suppress formation of the dense globs of cold gas that we identify with galaxies. However, our further tests with high-resolution simulations showed that this suppression was a numerical artifact, not a physi-

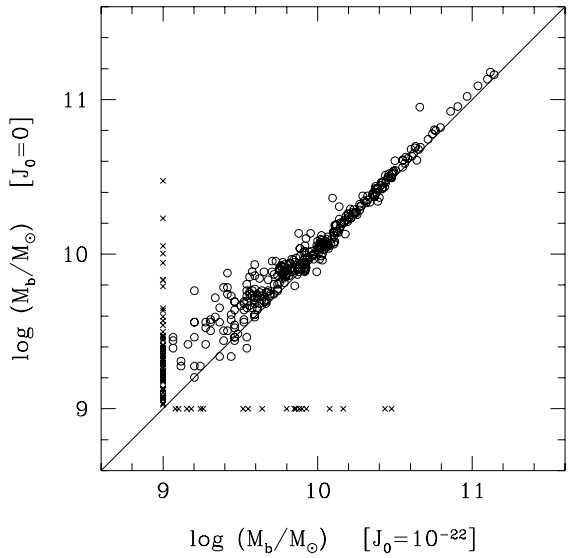

FIG. 8.—Galaxy-by-galaxy comparison of baryon masses from the high-resolution simulations with and without an ionizing background, at $z = 2$. The two galaxy lists are sorted in order of decreasing mass, and a galaxy from the photoionized simulation is matched to the first galaxy from the no-background simulation that has the same position to within 40 kpc and has not already been matched to a more massive galaxy. Circles represent matched galaxies, with mass in the no-background simulation plotted against mass in the photoionized simulation. Crosses show galaxies that were not matched. Of the 353 galaxies in the photoionized simulation, 334 find a match within 40 kpc.

cal effect. In this respect, our results tell a cautionary tale about the importance of numerical resolution in hydrodynamic cosmological simulations.

We interpret the qualitatively different outcomes between the low- and high-resolution simulations as follows. In the low-resolution simulations, galaxies comprised of ~32–128 gas particles are only marginally resolved, so their gas densities are underestimated. When there is no background radiation field, the gas still reaches densities high enough to allow efficient cooling and condensation within dark matter halos. However, when the background radiation field is included, the cooling rates at fixed density are lower, and in most cases the (underestimated) gas density is no longer high enough to permit efficient cooling. Only systems containing more than ~128 gas particles, corresponding to a mass $M_b \sim 1.5 \times 10^{11}\ M_\odot$, can cool and form dense globs. The high-resolution simulations avoid this numerical artifact, at least in the original mass range, because systems with $M_b \sim 10^{11}\ M_\odot$ are represented by many more particles and their gas densities are estimated accurately.

In simulations like these, the interplay between the numerical resolution and microphysical modeling can be quite subtle. As shown by the comparisons in Figures 6 and 7, for some purposes a low-resolution simulation *without* photoionization can be more realistic than a low-resolution simulation with a background radiation field, even though the latter has a more complete representation of the relevant microphysics. To make this point more clearly, we have repeated the galaxy matching analysis used to make Figure 8, but now we compare the baryonic masses of galaxies in the high-resolution simulation *with* an ionizing background to those in the low-resolution simulation *without* a radiation field. Because of the greater differences between the two simulations, we relax the position matching constraint from 40 kpc to 500 kpc. Figure 9*a* shows the baryonic mass comparison, and Figure 9*b* plots the distribution of separations of the matched galaxy pairs.

Figure 9 demonstrates several important features of these two simulations. First, only one of the 31 galaxies in the low-resolution case is not matched to a galaxy within 500 kpc in the other model. Second, all of the highest mass galaxies in the high-resolution simulation are matched to galaxies in the low-resolution calculation. Third, the typical shift in position between matched pairs is ~200 kpc. Finally, the masses of the galaxies in the matched pairs are in quite good agreement. The low-resolution simulation

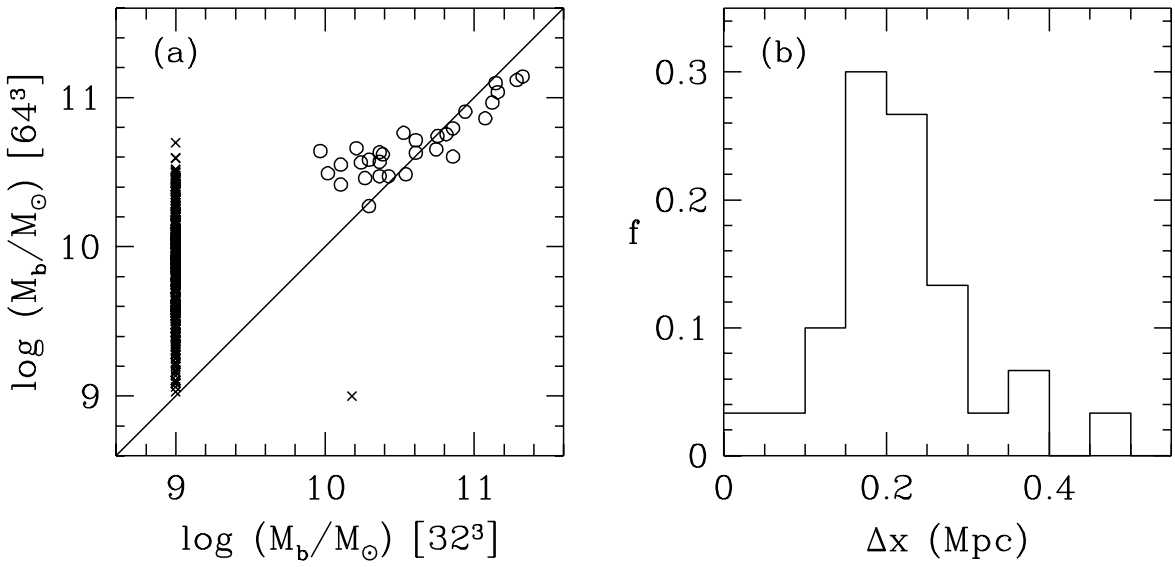

FIG. 9.—(*a*) Galaxy-by-galaxy comparison of baryon masses from the high-resolution simulation with an ionizing background and the low-resolution simulation with no radiation field, at $z = 2$. The procedure used to match galaxies in the two simulations is identical to that described in Fig. 8, except that the results here employ a larger matching distance of 500 kpc. Circles again represent matched galaxies, with mass in the high-resolution simulation plotted against mass in the low-resolution simulation. Crosses show galaxies that were not matched. Of the 31 galaxies in the low-resolution simulation, only one does not have a match within 500 kpc in the high-resolution run. (*b*) Distribution of three-dimensional distances between the matched galaxy pairs

yields slightly larger masses for the high-mass galaxies, probably because it creates a single glob out of material that at high resolution breaks into a dominant system with small satellites. It yields slightly smaller masses for the low-mass galaxies, probably because it underestimates the gas density and amount of cooling in the most poorly resolved objects.

From the galaxy distributions in Figure 6, it is obvious that the low-resolution simulations *with* an ionizing background would be a much worse match to their high-resolution counterparts, as there would be only a handful of galaxies to match. For a study of the galaxy population, the low-resolution simulation without photoionization gives much more realistic results. It is partly because of this complex interplay between microphysics and numerical resolution that we choose to treat the photoionizing background as an externally specified input to our simulations, instead of attempting to compute it self-consistently as done by Cen & Ostriker (1993).

One objective of hydrodynamic cosmological simulations is to predict the clustering of galaxies and the "bias" between galaxies and dark matter directly from *ab initio* theories of structure formation (e.g., Cen & Ostriker 1992; KHW; Evrard, Summers, & Davis 1994). A major obstacle to this program is the difficulty of simulating large, statistically representative cosmic volumes in reasonable amounts of computer time, while maintaining the resolution needed to follow cooling and condensation on galactic scales. This difficulty becomes acute if the high resolution used here in our 64^3 simulations is necessary to allow reliable identification of galaxies. However, the good agreement in spatial positions of massive objects quantified in Figure 9*b* indicates that a simulation with the resolution of our 32^3 runs and *no* ionizing background can yield accurate predictions for the clustering of luminous galaxies. If this conclusion is confirmed with simulations evolved to $z = 0$, then low-resolution calculations without photoionization can be used to study spatial clustering in a large volume. Figure 7 suggests that such simulations could also provide reasonable estimates of the high end of the baryonic mass function, although for detailed studies of the physics of galaxy formation it is probably better to sacrifice simulation volume in favor of high resolution and more complete microphysics.

For studies of Lyα absorption by diffuse intergalactic gas (Cen et al. 1994; Zhang, Anninos, & Norman 1995; Hernquist et al. 1996), it is essential to include a UV background because the gas that produces low column density absorption is highly photoionized. The UV background does not influence the dynamics of this gas, but it does determine its temperature and its neutral hydrogen fraction. One cannot obtain accurate absorption results from a simulation with no UV background by photoionizing it after the fact because the recombination rate (and hence the neutral fraction) depends on temperature, $\alpha \propto T^{-0.7}$. However, diffuse gas in our simulations with a UV background obeys a fairly tight correlation between density and temperature (see Fig. 3), so it might be possible to impose such a relation on a no-background simulation and thereby carry out Lyα analysis as a purely "postprocessing" step.

If we adopt 32 SPH particles as a nominal mass resolution limit, then the smallest resolved galaxies in our high-resolution simulations have a total (baryonic + dark) mass of $20 \times 32 \times 1.5 \times 10^8 \sim 10^{11}\ M_\odot$. In the spherical collapse model, a perturbation with this mass and a collapse redshift $z = 2$ (where our simulations stop) has a circular velocity $v_c \approx 100$ km s^{-1} (see TW, eq. [10]). Our simulations indicate that photoionization has little or no influence on the efficiency of galaxy formation down to this circular velocity; the small differences between our simulations with and without a UV background are probably the residual effect of finite numerical resolution.

Our conclusions about the impact of photoionization are consistent with those of Steinmetz (1995), QKE, and TW, all of whom examined collapses of individual objects with resolution higher than that used here. QKE performed three-dimensional simulations using TreeSPH, for a CDM model similar to that studied in this paper, but with $\sigma_8 = 0.5$ instead of 0.7 and a UV background intensity $J \approx 5 \times 10^{-21}$ ergs s^{-1} cm^{-2} sr^{-1} Hz^{-1}. TW used a one-dimensional code to simulate collapses of density peaks in spherical symmetry, at very high resolution, with a variety of parameters for the intensity, spectral shape, and evolution history of the UV background. The two studies reached remarkably similar conclusions: photoionization suppresses the formation of systems with $v_c \lesssim 35$ km s^{-1}, reduces the amount of cooled gas by about 50% for $v_c \approx 50$ km s^{-1}, and has progressively less effect toward higher circular velocities. The agreement between the two studies indicates that TW's results are not sensitive to their idealized geometry and that QKE's results are not sensitive to their choice of UV background parameters or to their finite resolution. The simulations in this paper, which represent a much larger comoving volume, cannot resolve systems of such low circular velocities, but they do show that no surprising new photoionization effects come into play during the hierarchical assembly of more massive galaxies.

Taken together, these studies suggest that photoionization alone will not solve the problem of excessive numbers of faint galaxies in the CDM model. Kauffmann, Guideroni, & White (1994), for example, find that star formation must be suppressed in halos with circular velocities up to 100 km s^{-1} in order to achieve acceptable agreement with observations. As an alternative to photoionization by the ambient UV background, one can appeal to local feedback within star-forming systems (Dekel & Silk 1986; White & Frenk 1991; Cole et al. 1994; Heyl et al. 1995). This mechanism can produce acceptable luminosity functions, but only if feedback suppresses the cooling of infalling gas very efficiently, perhaps unrealistically so. A third possibility, hinted at by a variety of recent studies (e.g., Marzke, Huchra, & Geller 1994; De Propris et al. 1995; Ferguson & McGaugh 1995) is that large numbers of faint galaxies are present in the real universe but are undercounted in conventional estimates of the luminosity function. Finally, there is the possibility that our current theoretical pictures of galaxy and structure formation are missing an important basic ingredient.

For $v_c > 100$ km s^{-1}, Figures 6–8 show that simulations with sufficient numerical resolution yield similar galaxy populations with and without a UV background. In Figure 10, we show that this robustness to microphysical assumptions holds more broadly. Panel (*a*), repeated from Figure 6, displays the galaxy distribution at $z = 2$ from the high-resolution simulation with $J_0 = 10^{-22}$ and $\alpha = 1$. Panel (*b*) shows a simulation that has the same initial conditions and UV background and includes star formation, using the algorithm described in KWH. Galaxies are identified by applying SKID to the combined distribution of star par-

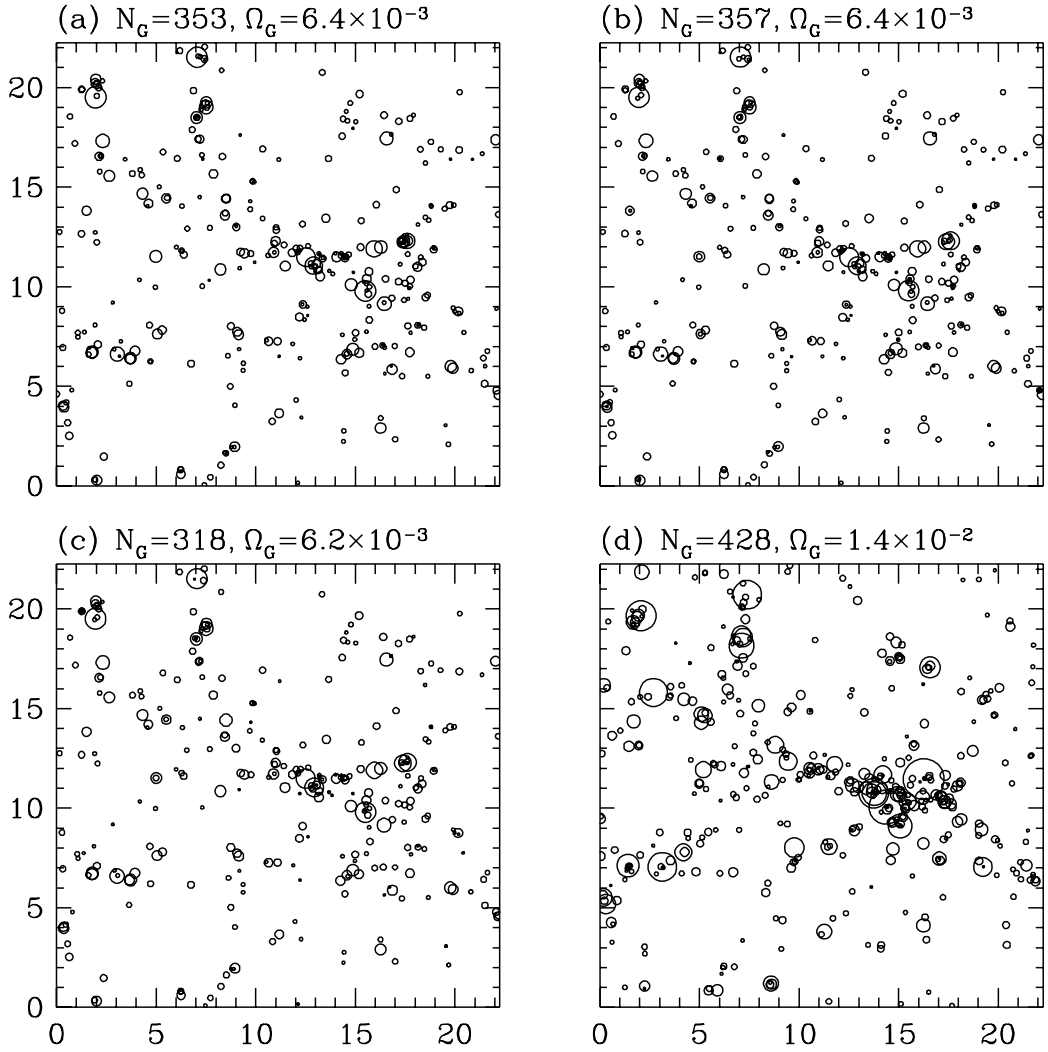

FIG. 10.—Galaxy distributions at $z = 2$ from (*a*) the high-resolution, photoionized simulation illustrated in Figs. 6–9, (*b*) a simulation with the same initial conditions and UV background but including star formation and feedback, (*c*) a simulation with the same initial conditions and star formation but a UV background spectrum taken from Haardt & Madau (1996), and (*d*) a simulation with star formation, the Haardt-Madau background, and initial conditions normalized to $\sigma_8 = 1.2$. Galaxy baryon masses (represented by circle areas on the same scale as in Fig. 4) include the contributions from stars and cold, dense gas. The first three simulations have the same initial conditions and yield similar galaxy populations despite their different treatments of microphysics. The fourth simulation has a higher fluctuation amplitude and produces more massive galaxies.

ticles and cold, dense gas particles ($\rho_b/\bar{\rho}_b > 1000$, $T < 30{,}000$ K); the area of the circle representing a galaxy indicates its mass of stars plus cold, dense gas. The galaxy populations are nearly identical even though the first simulation treats the baryon component hydrodynamically throughout the calculation and the second simulation steadily converts cold, dense gas into collisionless particles and injects thermal energy from supernova feedback into the surrounding medium. Figure 5 of KWH demonstrates similar insensitivity to assumptions about star formation in low-resolution simulations with no UV background evolved to $z = 0$.

The simulations illustrated in Figures 10*a* and 10*b* both assume a simple ν^{-1} spectrum for the UV background. Figure 10*c* shows a simulation with star formation and the UV background spectrum of Haardt & Madau (1996), who compute the ambient radiation field that would be produced by the observed population of quasars after absorption and re-emission by the Lyα forest. We use their spectra for $q_0 = 0.5$ (kindly provided by P. Madau) to compute photoionization parameters and photoionization heating parameters as a function of redshift (see § 3 of KWH for formal definitions of these quantities). We reduce the amplitude of the spectrum by a factor of 2 so that the simulation roughly reproduces the observed mean Lyα opacity toward high-z quasars (Press, Rybicki, & Schneider 1993) for our adopted baryon density of $\Omega_b = 0.05$. Despite the changes in the spectral shape, intensity, and evolution of the UV background, the galaxy population in Figure 10*c* is almost indistinguishable from that in Figure 10*b*, except for the absence of a few of the smallest systems. The assumed UV background does influence the amount of Lyα absorption produced by intergalactic hydrogen, but the effect enters mainly through a single parameter, the background intensity weighted by photoionization cross section ($\Gamma_{\gamma H_0}$ in the notation of KWH).

Figure 10*d* shows the galaxy population from a similar CDM model but with the power spectrum normalized to $\sigma_8 = 1.2$, close to the level implied by *COBE*. We again incorporate star formation and the Haardt & Madau (1996)

ionizing background spectrum. While the overall structure of the galaxy distribution is similar in this simulation (the initial fluctuations were increased in amplitude but otherwise unaltered), the largest galaxies are considerably more massive. There are also a number of low mass galaxies present in this model that have not formed by this redshift in the lower normalization simulation. The galaxy mass functions for the three $\sigma_8 = 0.7$ simulations are nearly identical, but the mass function for the $\sigma_8 = 1.2$ simulation is shifted systematically toward higher masses.

Our results show that numerical resolution is important for studying galaxy formation in simulations like these and that the required resolution can depend on the microphysical treatment in a complicated way. They also suggest that there are critical regimes where a small change in resolution can produce a major, qualitative change in results, by shifting a simulation from a regime where gas in a typical halo can cool to a regime where it cannot. Figure 10 adds an encouraging coda to this disconcerting story: when the numerical resolution is adequate, the simulated galaxy population is insensitive to uncertain microphysical assumptions, at least within the range that we have examined here. The one model that stands out in Figure 10 is the one with a different primordial fluctuation amplitude, and it is easily distinguished from the others. Simulations that model galaxy formation in a large volume to $z = 0$ will be computationally demanding, but we can expect them to provide good constraints on theories of the origin of cosmic structure.

We acknowledge valuable discussions with Jeremiah Ostriker, Tom Quinn, Martin Rees, Anne Thoul, and Simon White. We thank Piero Madau for providing us with the Haardt & Madau (1996) UV background spectrum and for helpful discussions about the UV background. We thank Gus Evrard for a helpful referee's report. This work was supported in part by the Pittsburgh Supercomputing Center, the National Center for Supercomputing Applications (Illinois), the San Diego Supercomputing Center, the Alfred P. Sloan Foundation, a Hubble Fellowship (N. S. K.), NASA theory grants NAGW-2422, NAGW-2523, and NAG 5-2882, NASA HPCC/ESS grant NAG 5-2213, and the NSF under grants AST 90-18526, ASC 93-18185, and the Presidential Faculty Fellows Program. D. H. W. acknowledges the support of a Keck fellowship at the Institute for Advanced Study during part of this work.

REFERENCES

Babul, A., & Rees, M. J. 1992, MNRAS, 255, 346
Barnes, J. E., & Hut, P. 1986, Nature, 324, 446
Black, J. H. 1981, MNRAS, 197, 553
Blanchard, A., Valls-Gabaud, D., & Mamon, G. A. 1992, A&A, 264, 365
Blumenthal, G. R., Faber, S. M., Primack, J. R., & Rees, M. J. 1984, Nature, 311, 517
Bouchet, F. R., & Hernquist, L. 1988, ApJS, 68, 521
Bunn, E. F., Scott, D., & White, M. 1995, ApJ, 441, L9
Cen, R. 1992, ApJS, 78, 341
Cen, R., Miralda-Escudé, J., Ostriker, J. P., & Rauch, M. 1994, ApJ, 437, L9
Cen, R., & Ostriker, J. P. 1992, ApJ, 399, L113
———. 1993, ApJ, 417, 404
Cole, S. 1991, ApJ, 367, 45
Cole, S., Aragon-Salamanca, A., Frenk, C. S., Navarro, J. F., & Zepf, S. E. 1994, MNRAS, 271, 744
Dekel, A., & Silk, J. 1986, ApJ, 303, 39
De Propris, R., Pritchet, C. J., Harris, W. E., & McClure, R. D. 1995, ApJ, 450, 534
Efstathiou, G. 1992, MNRAS, 256, L43
Evrard, A. E. 1988, MNRAS, 235, 911
Evrard, A. E., Summers, F. J., & Davis, M. 1994, ApJ, 422, 11
Ferguson, H. C., & McGaugh, S. S. 1995, ApJ, 440, 470
Gelb, J. M., & Bertschinger, E. 1994a, ApJ, 436, 467
———. 1994b, ApJ, 436, 491
Gingold, R. A., & Monaghan, J. J. 1977, MNRAS, 181, 375
Haardt, F., & Madau, P. 1996, ApJ, 461, 20
Hernquist, L. 1987, ApJS, 64, 715
Hernquist, L., Bouchet, F. R., & Suto, Y. 1991, ApJS, 75, 231
Hernquist, L., & Katz, N. 1989, ApJS, 70, 419
Hernquist, L., Katz, N., & Weinberg, D. H. 1995, ApJ, 442, 57
Hernquist, L., Katz, N., Weinberg, D. H., & Miralda-Escudé, J. 1996, ApJ, 457, L51
Heyl, J. S., Cole, S., Frenk, C. S., & Navarro, J. F. 1995, MNRAS, 274, 755
Ikeuchi, S. 1986, Ap&SS, 118, 509
Katz, N., Hernquist, L., & Weinberg, D. H. 1992, ApJ, 399, L109 (KHW)
Katz, N., Weinberg, D. H., & Hernquist, L. 1996, ApJS, 105, 19 (KWH)
Kauffmann, G., Guideroni, B., & White, S. D. M. 1994, MNRAS, 267, 981
Kauffmann, G., White, S. D. M., & Guideroni, B. 1993, MNRAS, 264, 201
Lacey, C. G., & Silk, J. 1991, ApJ, 381, 14
Lucy, L. 1977, AJ, 82, 1013
Marzke, R. O., Huchra, J. P., & Geller, M. J. 1994, ApJ, 428, 43
Miralda-Escudé, J., & Ostriker, J. P. 1992, ApJ, 392, 15
Monaghan, J. J. 1992, AR&A, 30, 543
Navarro, J., & Steinmetz, M. 1996, ApJ, in press
Peebles, P. J. E. 1982, ApJ, 263, L1
Press, W. H., Rybicki, G., & Schneider, D. P. 1993, ApJ, 414, 64
Press, W. H., & Schechter, P. 1974, ApJ, 187, 425
Quinn, T. R., Katz, N., & Efstathiou, G. 1996, MNRAS, 278, L49 (QKE)
Rees, M. J. 1986, MNRAS, 218, L25
Smoot, G., et al. 1992, ApJ, 396, L1
Steinmetz, M. 1995, in Ann. NY Acad. Sci. 759, Proc. 17th Texas Symp. Relativistic Astrophysics, 628
Tegmark, M., Silk, J., & Evrard, A. E. 1993, ApJ, 417, 54
Thoul, A. A., & Weinberg, D. H. 1996, ApJ, 465, 608 (TW)
Vedel, H., Hellsten, U., & Sommer-Larsen, J. 1994, MNRAS, 271, 743
White, S. D. M., Efstathiou, G., & Frenk, C. S. 1993, MNRAS, 262, 1023
White, S. D. M., & Frenk, C. S. 1991, ApJ, 379, 52
White, S. D. M., & Rees, M. J. 1978, MNRAS, 183, 341
Zhang, Y., Anninos, P., & Norman, M. L. 1995, ApJ, 453, L57